Acta Crystallographica Section F
Structural Biology and Crystallization Communications
ISSN 1744-3091

Structural insights into RipC, a putative citrate lyase β subunit from a *Yersinia pestis* virulence operon

Rodrigo Torres,[a] Nicholas Chim,[a] Banumathi Sankaran,[b] Céline Pujol,[c]‡ James B. Bliska[c] and Celia W. Goulding[a,d]*

[a]Department of Molecular Biology and Biochemistry, University of California, Irvine, CA 92697, USA, [b]Berkeley Center for Structural Biology, Lawrence Berkeley National Laboratory, Berkeley, CA 94720, USA, [c]Department of Molecular Genetics and Microbiology and Center for Infectious Diseases, State University of New York, Stony Brook, NY 11794, USA, and [d]Department of Pharmaceutical Sciences, University of California, Irvine, CA 92697, USA

‡ Present address: DGA Maîtrise NRBC, Le Bouchet, BP3, 91710 Vert-le-Petit, France.

Correspondence e-mail: celia.goulding@uci.edu

Received 30 August 2011
Accepted 11 November 2011

PDB Reference: RipC, 3qll.

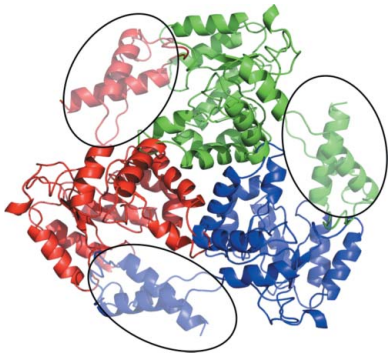

Yersinia pestis remains a threat, with outbreaks of plague occurring in rural areas and its emergence as a weapon of bioterrorism; thus, an improved understanding of its various pathogenicity pathways is warranted. The *rip* (required for intracellular proliferation) virulence operon is required for *Y. pestis* survival in interferon-γ-treated macrophages and has been implicated in lowering macrophage-produced nitric oxide levels. RipC, one of three gene products from the *rip* operon, is annotated as a citrate lyase β subunit. Furthermore, the *Y. pestis* genome lacks genes that encode citrate lyase α and γ subunits, suggesting a unique functional role of RipC in the *Y. pestis rip*-mediated survival pathway. Here, the 2.45 Å resolution crystal structure of RipC revealed a homotrimer in which each monomer consists of a $(\beta/\alpha)_8$ TIM-barrel fold. Furthermore, the trimeric state was confirmed in solution by size-exclusion chromatography. Through sequence and structure comparisons with homologous proteins, it is proposed that RipC is a putative CoA- or CoA-derivative binding protein.

1. Introduction

The *Yersinia* genus consists of three human pathogens. The most deadly, *Y. pestis*, has been responsible for three major pandemics of bubonic plague throughout history. Although current antibiotics are effective against the disease, *Y. pestis* infection, which occurs mostly in rural areas, can still result in illness and death. More alarmingly, *Y. pestis* has emerged as a biological weapon, especially in light of its propensity to evolve multidrug resistance. Additionally, two enteropathogens, *Y. pseudotuberculosis* and *Y. enterocolitica*, cause a broad range of gastrointestinal diseases (Butler, 2009). Thus, understanding the mechanisms of *Yersinia* pathogenesis is important.

Although its extracellular pathogenicity has been well established (Heesemann *et al.*, 2006), *Y. pestis* is a facultative intracellular pathogen that is capable of surviving and replicating in macrophages. Interestingly, *Y. pestis* has been shown to replicate in interferon-γ (INF-γ) treated (post-activated) macrophages, which is coupled with a reduction of toxic nitric oxide (NO) levels even though macrophage-inducible NO synthase (iNOS) is up-regulated by INF-γ (Pujol *et al.*, 2005). Furthermore, a *Y. pestis* mutant with its pigmentation locus deleted does not survive in post-activated wild-type macrophages but is able to replicate in post-activated iNOS$^{-/-}$ macrophages, suggesting that killing of this mutant is NO-dependent. The presence of two genes, *ripA* and *ripB*, have further been demonstrated to be important for *Y. pestis* survival, as well as restriction of macrophage NO levels, implicating that the *ripA* and *ripB* gene products are directly or indirectly responsible for lowering macrophage-produced NO levels (Pujol *et al.*, 2005). Thus, *ripA* and *ripB*, together with a third gene y2383 (designated *ripC*), form a novel virulence operon designated *rip* (**r**equired for **i**ntracellular **p**roliferation) that is essential for intracellular replication of *Y. pestis* in post-activated macrophages (Pujol *et al.*, 2005).

In order to investigate the novel *rip* operon at a molecular level, we present the 2.45 Å resolution crystal structure of the product of the first gene in the operon, RipC, which is annotated as a citrate lyase β subunit. Within eukaryotes, ATP-dependent citrate lyases are single polypeptide chains that convert citrate to acetyl-CoA and

oxaloacetate (Kanao *et al.*, 2002), where acetyl-CoA is eventually used in fatty-acid metabolism. Prokaryotes have a similar Mg^{2+}-dependent albeit ATP-independent process facilitated by a complex composed of α and β catalytic subunits and a γ acyl carrier protein (ACP) subunit (Schneider *et al.*, 2002). *Y. pestis* RipC is homologous to the β subunit, which, in the context of bacterial citrate lyase, catalyzes the conversion of citryl-CoA-ACP to acetyl-CoA-ACP and oxaloacetate (Bott & Dimroth, 1994). Interestingly, *Y. pestis*, along with a subset of other pathogenic bacteria and higher metazoans, lacks the α and γ subunits of the prokaryotic citrate lyase complex, dictating a distinct biochemical function (Goulding *et al.*, 2007). Based on sequence and structure comparisons with other bacterial citrate lyase β subunits, as well as with a homologous halophilic archaeal malate synthase, we identify a conserved trimeric assembly as well as RipC residues that constitute a putative CoA-binding site. Therefore, RipC could play a role in the *rip*-mediated pathogenicity pathway by providing a precursor CoA derivative which can be directly or indirectly utilized by RipA, a putative butyryl-CoA transferase (Torres *et al.*, 2011), or/and RipB, an annotated enoyl-CoA hydrolase.

2. Materials and methods

2.1. Protein expression and purification

To construct a *ripC* expression plasmid, the *ripC* ORF was amplified by PCR using chromosomal DNA from *Y. pestis* strain KIM6+ as a template and the primers ripC-*Eco*RI (5′-cggaattcATGTCTAATCTTGATACTTACCAAACCCGCA-3′) and ripC-*Xba*I (5′-gctctagaTCAGGCAGAGATACCCGCTCGGGTAAGTACC-3′). The PCR product was inserted into the *Eco*RV site of pETBlue-2 using the Perfectly Blunt cloning kit (Novagen). The resulting plasmid was subsequently digested by *Eco*RI and *Sac*I and the *Eco*RI–*Sac*I DNA fragment containing *ripC* was isolated and inserted into pET-28 using *Eco*RI and *Sac*I restriction sites. The resulting pET-28-*ripC* plasmid expresses the full-length RipC protein with an N-terminal 6×His tag and additional non-native linker residues (*i.e.* SSGLVPRGSHMASMTGGQQMGRGSEF), with a corresponding molecular weight of 33.4 kDa. *Escherichia coli* BL21-Gold(DE3) cells harbouring pET-28-*ripC* were grown aerobically at 310 K in LB medium containing 30 µg ml^{-1} kanamycin. RipC expression was induced with 1 m*M* isopropyl β-D-1-thiogalactopyranoside at an $OD_{600\,nm}$ of ∼1.0 and cells were harvested after 4 h by centrifugation at 5000 rev min^{-1} for 10 min and then resuspended in wash buffer (50 m*M* Tris pH 7.4, 350 m*M* NaCl, 10 m*M* imidazole) containing phenylmethylsulfonyl fluoride (PMSF) and hen egg-white lysozyme. The cells were lysed by sonication on ice and centrifuged at 13 000 rev min^{-1} for 40 min. The cell lysate was filtered (1 µm) to remove cell debris, loaded onto an Ni^{2+}-charged HiTrap column (5 ml) and washed with wash buffer. Fractions of eluted protein (between 200 and 300 m*M* imidazole) were collected and concentrated (Amicon, 10 kDa molecular-mass cutoff) to 7 mg ml^{-1}. Selenomethionine-derivatized (SeMet) RipC was expressed in M9 minimal medium supplemented with amino acids (leucine, isoleucine and valine at 50 mg l^{-1}, phenylalanine, lysine and threonine at 100 mg l^{-1} and selenomethionine at 75 mg l^{-1}; Van Duyne *et al.*, 1993) and purified similarly to native RipC.

2.2. Crystallization, data collection and processing

Native and SeMet RipC crystals were grown by the hanging-drop vapour-diffusion method using a reservoir consisting of 18%(*v*/*v*) ethylene glycol and 0.1 *M* tris(2-carboxyethyl)phosphine at room temperature; crystals grew after 1–5 d. Cryoloops containing crystals were swiped through mother liquor containing 25%(*v*/*v*) glycerol as a cryoprotectant and cooled in liquid nitrogen; data were collected at 100 K. SeMet RipC crystallized in space group $P3_121$, with unit-cell parameters $a = b = 88.05$, $c = 197.02$ Å, and contained three molecules per asymmetric unit. Two data sets (*i.e.* 2.6 and 2.45 Å) were collected from a single SeMet crystal on beamline 5.0.2 at the Advanced Light Source (ALS); the 2.6 Å single-wavelength anomalous dispersion (SAD) data set was collected at 0.9787 Å as determined from a fluorescence scan (Se absorption-edge energy of 12 668.7 eV, $f' = -7.8$, $f'' = 4$). Data reduction for both data sets was carried out with the *HKL*-2000 suite (Otwinowski & Minor, 1997), resulting in at least 99% complete data sets (Table 1).

Table 1
X-ray diffraction data-collection and atomic refinement statistics for *Y. pestis* RipC.

Values in parentheses are for the highest resolution shell.

	SeMet (2.6 Å)	SeMet (2.45 Å)
Space group	$P3_121$	$P3_121$
Unit-cell parameters (Å)	$a = b = 88.05$, $c = 197.02$	$a = b = 88.05$, $c = 197.02$
pH of crystallization condition	7.4	7.4
Protein concentration (mg ml^{-1})	7	7
Data set		
Wavelength (Å)	0.9787	0.9789
Resolution range (Å)	50–2.60 (2.74–2.60)	50–2.45 (2.52–2.45)
Total reflections	289597	423287
Unique reflections	28096	33335
Completeness (%)	99.0 (100)	99.1 (100)
Multiplicity	12.8 (12.1)	6.8 (6.6)
R_{merge}† (%)	7.2 (60.8)	7.1 (51.7)
R_{meas}‡ (%)	7.8 (66.3)	—
$R_{p.i.m.}$§ (%)	2.3 (18.7)	—
R_{anom}¶ (%)	3.0 (26.0)	—
$\langle I/\sigma(I)\rangle$	22.2 (4.2)	28.8 (5.75)
FOM	0.34	—
No. of Se sites	9	—
NCS copies	3	3
Model refinement		
Resolution range (Å)		42.96–2.45
No. of reflections (working/free)		32907/2013
No. of protein atoms		4746
No. of water molecules		27
Missing residues		1–4, 20–29, 57–65, 119–120, 241–280
R_{work}/R_{free}†† (%)		23.0/25.6
R.m.s. deviations		
Bond lengths (Å)		0.012
Bond angles (°)		1.199
Ramachandran plot, residues in (%)		
Most favorable region		99.03
Additional allowed region		0.97
Disallowed region		0
PDB code		3qll

† $R_{merge} = \sum_i \sum |I_i - \langle I\rangle| / \sum_i \sum I_i$. ‡ $R_{meas} = \sum \{N/[N-1]\}^{1/2} \sum_i |I_i - \langle I\rangle| / \sum_i \sum I_i$. § $R_{p.i.m.} = \sum \{1/[N-1]\}^{1/2} \sum_i |I_i - \langle I\rangle| / \sum_i \sum I_i$. ¶ $R_{anom} = \sum \sum_i |I_i - \langle I\rangle| / \sum \sum_i \langle I\rangle$. †† $R_{work} = \sum ||F_{obs}| - |F_{calc}|| / \sum |F_{obs}|$. R_{free} was computed identically except all reflections belonged to a test set consisting of a 5% random selection of the data.

2.3. Structure determination, refinement and analysis

RipC structure determination and refinement was performed using the *PHENIX* suite of programs (Adams *et al.*, 2010). Initial phases were determined from the 2.6 Å resolution data set using *AutoSol*, which located nine Se sites. Model building was then performed with a combination of automated building utilizing *AutoBuild*, in which initial density modification improved the electron-density maps, and manual building using *Coot* (Emsley *et al.*, 2010). Phases were extended to 2.45 Å resolution using the high-resolution data set and the model was refined using *phenix.refine*, yielding final R and R_{free} values of 23.0% and 25.6%, respectively, by employing NCS

restraints and TLS parameters followed by refinement of waters and optimization of X-ray/stereochemistry weighting (Table 1). The relatively high R and R_{free} are comparable to those reported for other citrate lyase β subunit crystal structures with unresolved C-terminal regions, *i.e.* those from *Mycobacterium tuberculosis* (PDB entry 1u5h; R = 26.8%, R_{free} = 27.2%; Goulding *et al.*, 2007) and *Deinococcus radiodurans* (PDB entry 1sgj; R = 22.7%, R_{free} = 24.3%; New York SGX Research Center for Structural Genomics, unpublished work). The stereochemistry and geometry was validated with *PROCHECK* (Laskowski *et al.*, 1993) and *MolProbity* (Chen *et al.*, 2010). The final 2.45 Å resolution model coordinates and structure factors have been deposited in the PDB as entry 3qll. All molecular graphics were prepared with *PyMOL* (DeLano, 2002).

2.4. Size-exclusion chromatography

A Superdex 200 10/60 column (GE Healthcare) was used to determine the oligomeric state of RipC. 500 µl RipC was loaded onto the column at 1 ml min^{-1} using an ÄKTA FPLC system. The oligomeric state of RipC was evaluated according to protein standards (Bio-Rad); a calibration curve was determined by plotting the K_{av} of the protein standards against the log MW of the protein standards. K_{av} was calculated using the equation $K_{av} = (V_e - V_0)/(V_t - V_0)$, where V_e is the standard elution volume, V_0 (40 ml) is the void volume and V_t (120 ml) is the total volume.

3. Results and discussion

3.1. Overall RipC structure

The RipC crystal structure contains three monomers per asymmetric unit, with a threefold noncrystallographic symmetry axis. Each RipC monomer reveals a canonical $(\beta/\alpha)_8$ TIM barrel consisting of residues 11–152 and 167–232, with an additional helix (α6a; residues 154–161) that protrudes over the C-terminal end, or top, of the barrel (PDB entry 3qll; Fig. 1*a*). The final monomer model excludes the first predicted α-helix (residues 20–29) of the TIM barrel, the last 40

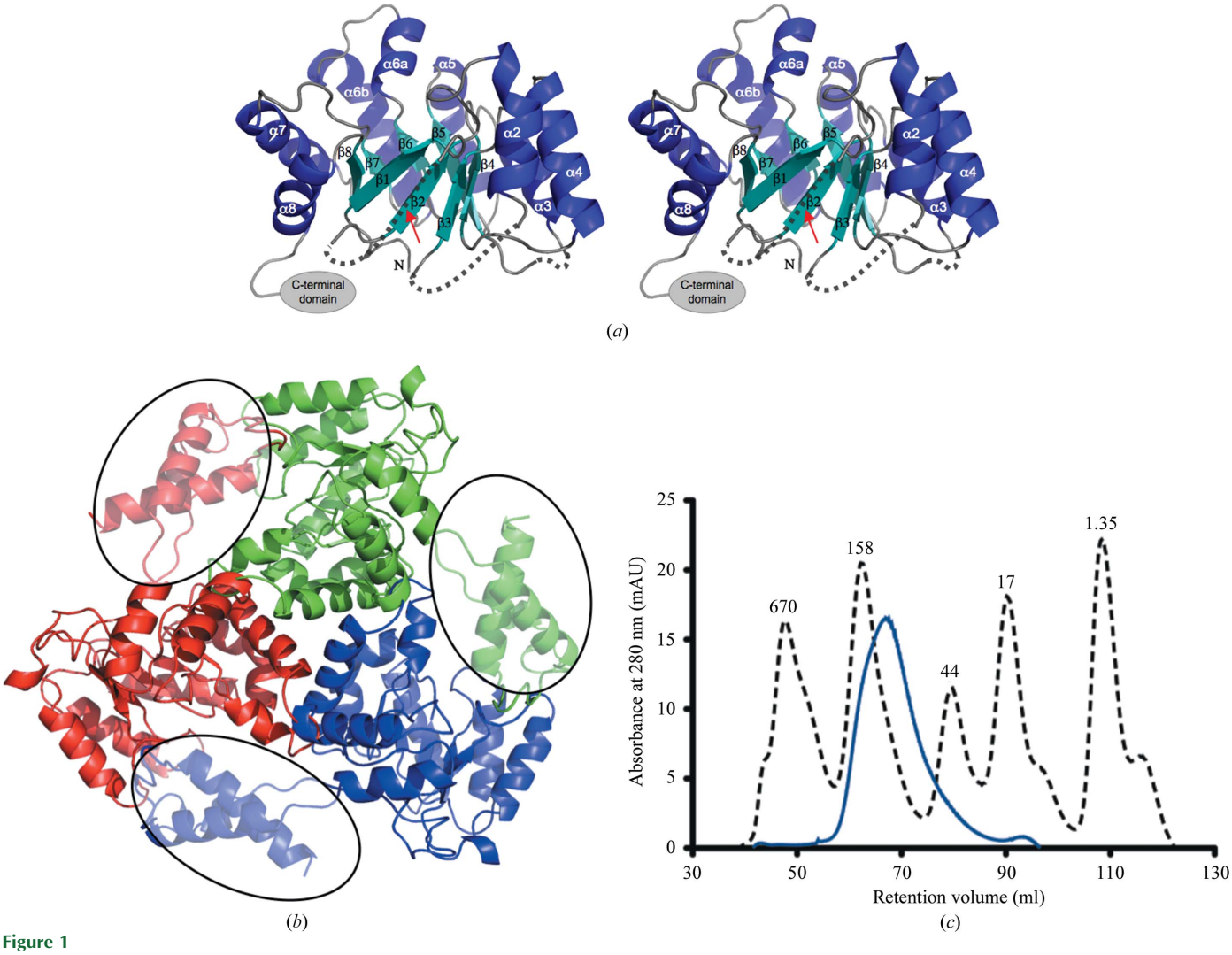

Figure 1
Structure of *Y. pestis* RipC. (*a*) Stereoview of monomeric RipC depicting the TIM barrel, in which the α-helices, β-strands and loops are colored blue, cyan and gray, respectively. Missing residues within the TIM-barrel domain, including α-helix 1 (indicated by a red arrow), are represented as dotted lines, whereas the C-terminal domain is represented as a gray oval. (*b*) Trimeric RipC with a homology model of the C-terminal unstructured domain based on the *I-Tasser* composite model (Roy *et al.*, 2010), in which the predicted topology of the C-terminal domains is circled and shaded and is located close to the top of the TIM barrel of an adjacent monomer. Monomers are colored blue, red and green. (*c*) The size-exclusion chromatogram reveals trimeric RipC (blue trace) based on protein calibration standards (black dashed trace; labelled in kDa).

residues of the C-terminal region and two loop regions (residues 57–65 and 119–120) owing to a lack of observable electron density (Fig. 1*a*). Furthermore, these unresolved regions are all located towards the N-terminal end, or bottom, of the TIM barrel despite predicted secondary-structure elements (Cole *et al.*, 2008) for α-helix 1 (α1) and the final C-terminal region (Figs. 1*a* and 2). The flexibility or unresolved nature of α1 could potentially be a consequence of the disordered 36-residue N-terminal linker or may require additional protein–protein/substrate interactions for stability.

Each RipC monomer interacts symmetrically with both adjacent monomers primarily through TIM-barrel α-helix 6b, forming a trimer that consists of a hydrophobic core with an approximate height of 75 Å and depth of 43 Å (Fig. 1*b*). Additional contacts contributed by loop residues between α-helices 6a and 7, as well as residues at the beginning of α-helix 5, further stabilize the RipC trimer. The total buried surface area per monomer is about 938 Å^2, corresponding to approximately 9% of the total surface area of 10 713 Å^2 (Lee & Richards, 1971). The positional r.m.s.d. (Krissinel & Henrick, 2007) of all 215 ordered C$^\alpha$ atoms among all three RipC monomers ranges between 0.27 and 0.60 Å, suggesting that there is no significant difference between the monomers within the trimer. The RipC oligomer observed in the crystal structure was further experimentally confirmed by size-exclusion chromatography (Fig. 1*c*); RipC elutes in a single peak at 67.3 ml (K_{av} = 2.05) corresponding to 112.2 kDa, which is close to the predicted trimer molecular weight of 100.2 kDa.

3.2. Sequence and structural comparisons

RipC is homologous to other annotated citrate lyase β subunits; in particular, RipC shares sequence identities of 33, 23, 20 and 19% with homologs that have structures deposited in the PDB from *M. tuberculosis* (CitE; PDB entry 1u5h), *D. radiodurans* (PDB entry 1sgj), *Burkholderia xenovorans* (PDB entry 3r4i; Joint Center for Structural Genomics, unpublished work) and *Ralstonia eutropha* (PDB entry 3qqw; Joint Center for Structural Genomics, unpublished work), respectively (Fig. 2). Apart from the alternating β/α topology

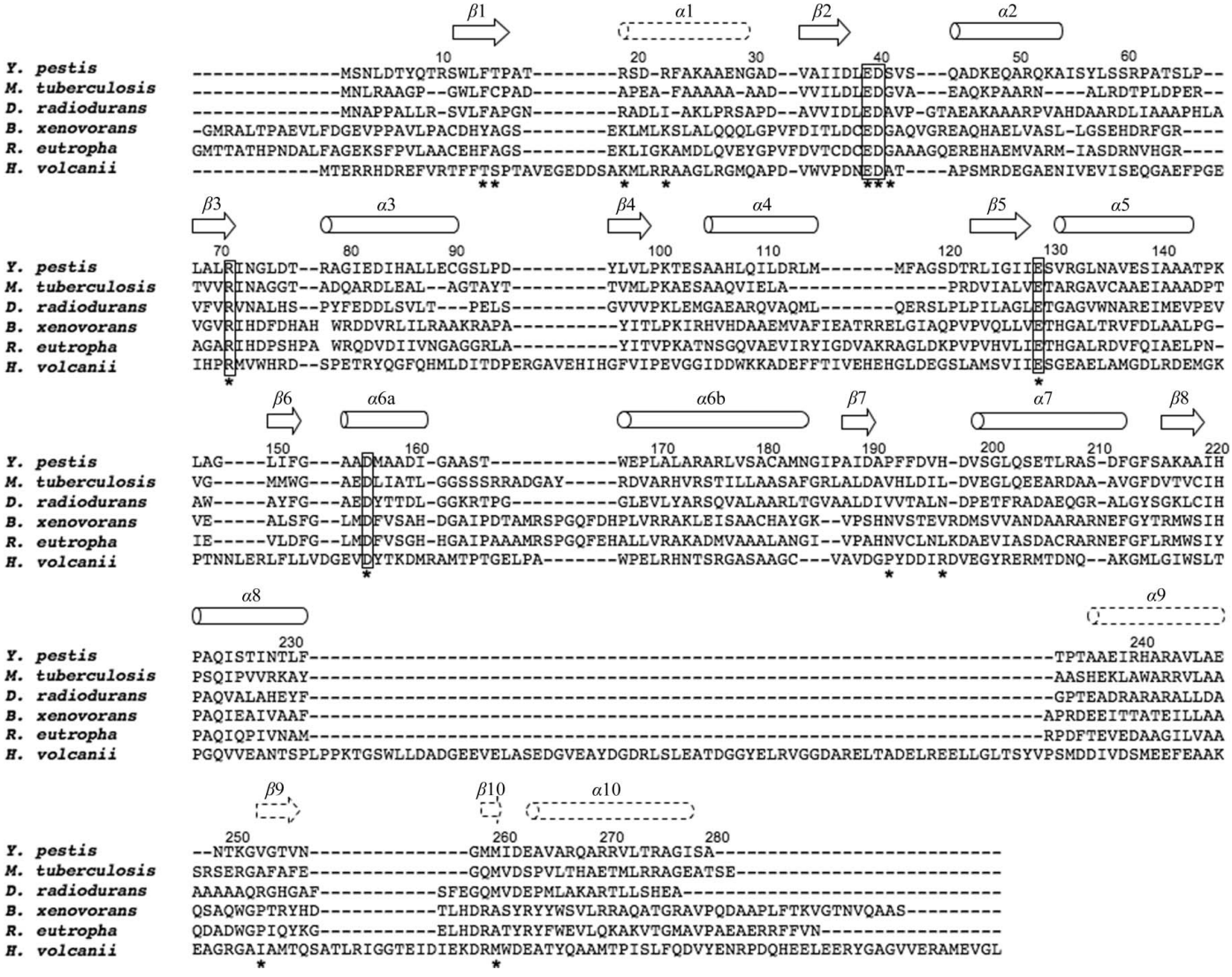

Figure 2
Sequence alignment of *Y. pestis* RipC with other citrate lyase β subunits (*M. tuberculosis* CitE, PDB entry 1u5h; *D. radiodurans*, PDB entry 1sgj; *B. xenovorans*, PDB entry 3r4i; *R. eutropha*, PDB entry 3qqw), as well as *H. volcanii* malate synthase H (PDB entry 3oyz; Bracken *et al.*, 2011). Cylinders and arrows define the regions of α-helices and β-strands, respectively. Dotted secondary-structure elements are predicted by *JPred* (Cole *et al.*, 2008) and represent regions missing in the RipC crystal structure. RipC residues that are proposed to interact with CoA or a CoA derivative, based on sequence conservation with *H. volcanii* malate synthase H, are indicated by asterisks; fully conserved residues are boxed.

of the TIM barrel, the final 40 residues (C-terminal domain) that are disordered in the RipC crystal structure based on secondary-structure prediction (Cole *et al.*, 2008) should putatively contain two α-helices and two β-strands (Fig. 2).

Structural comparison reveals that, as in RipC, all of the above-mentioned annotated citrate lyase β subunits share conserved subunit-interaction interfaces that lead to similar trimeric arrangements. Additionally, the C-terminal domain is also absent in the structures of citrate lyase β subunits from *M. tuberculosis* and *D. radiodurans*, which is suggestive of domain disorder, whereas the corresponding residues in *R. eutropha* are partially built, with two additional α-helices. Furthermore, the C-terminal domain from *B. xenovorans* is fully structured and exhibits a three-α-helical bundle capped by a β-turn, which makes no extensive contacts with its N-terminal TIM-barrel domain or with that of the adjacent subunit (Fig. 3*a*). Using the fully automated *I-Tasser* webserver (Roy *et al.*, 2010), a RipC homology model was built utilizing the full-length sequence and truncated structure (*i.e.* without the final 40 C-terminal residues) as initial restraints, as well as citrate lyase β subunits from *M. tuberculosis*, *D. radiodurans* and *B. xenovorans* as additional templates. The final assembled structures were subjected to iterative *ab initio* modeling and energy minimizations, resulting in a homology model which suggests that the C-terminal domain of one RipC subunit may interact with the top of the TIM barrel of an adjacent RipC subunit (Fig. 1*b*).

3.3. Putative active site

The ternary structure of malate synthase H (MSH) from *Haloferax volcanii* complexed with acetyl-CoA and pyruvate has recently been reported (Bracken *et al.*, 2011). Although sequence alignment revealed a relatively low identity of 10% (Fig. 2), RipC shares structural homology with MSH (1.81 Å r.m.s.d. over 196 RipC C^{α} atoms) that is comparable to that with *B. xenovorans* citrate lyase β subunit (1.74 Å r.m.s.d. over 202 RipC C^{α} atoms; Krissinel & Henrick, 2007). More importantly, MSH is trimeric and thus represents the first and most relevant acetyl-CoA-bound TIM-barrel structure that can be used to shed light on the putative ability of RipC to bind CoA derivatives. The active site of MSH consists of residues from the TIM barrel and the C-terminal domain (Fig. 3); however, owing to a stretch of approximately 40 missing residues connecting the two domains the active site may be formed through an intramonomer interaction, as shown in Fig. 3, or through an intermonomer interaction in which the C-terminal domain of one monomer caps the top of the TIM barrel from an adjacent monomer.

As previously observed in other malate synthase structures (Anstrom *et al.*, 2003; Smith *et al.*, 2003), acetyl-CoA adopts a bent conformation when bound to MSH. Superimposing the TIM barrels reveals that key active-site residues from MSH (Glu51, Asp52, Arg84, Glu158, Asp192 and Pro231) that are important in binding pyruvate and the acetate moiety of acetyl-CoA are highly conserved in RipC (Glu39, Asp40, Arg71, Glu129, Asp156 and Pro192) (Fig. 3). Furthermore, Phe1 in RipC (α-helix 1) may compensate for the absence of Trp257 (α-helix 8) in MSH. The corresponding residues are also conserved in *M. tuberculosis* citrate lyase β subunit (CitE), which binds oxaloacetate and magnesium (Goulding *et al.*, 2007). Interestingly, *M. tuberculosis* CitE also occurs in the absence of α and γ subunits, and Goulding and coworkers were the first to suggest that a lone *citE* gene encodes a protein that may function differently from a citrate lyase β subunit that occurs in the presence of α and γ subunits (Goulding *et al.*, 2007); thus, CitE and RipC may function analogously.

Additional hydrophobic MSH residues that stabilize the rest of acetyl-CoA are further conserved in RipC (Fig. 3). In particular, Ser17 and Ala53 of MSH, which interact with the pantothenate arm of CoA, correspond to Thr15 and Ser41 of RipC. Moreover, a positively charged pair of residues (Lys29 and Arg33; Fig. 3, expanded region) in MSH flank the phosphate group on the 3′ ribose of the

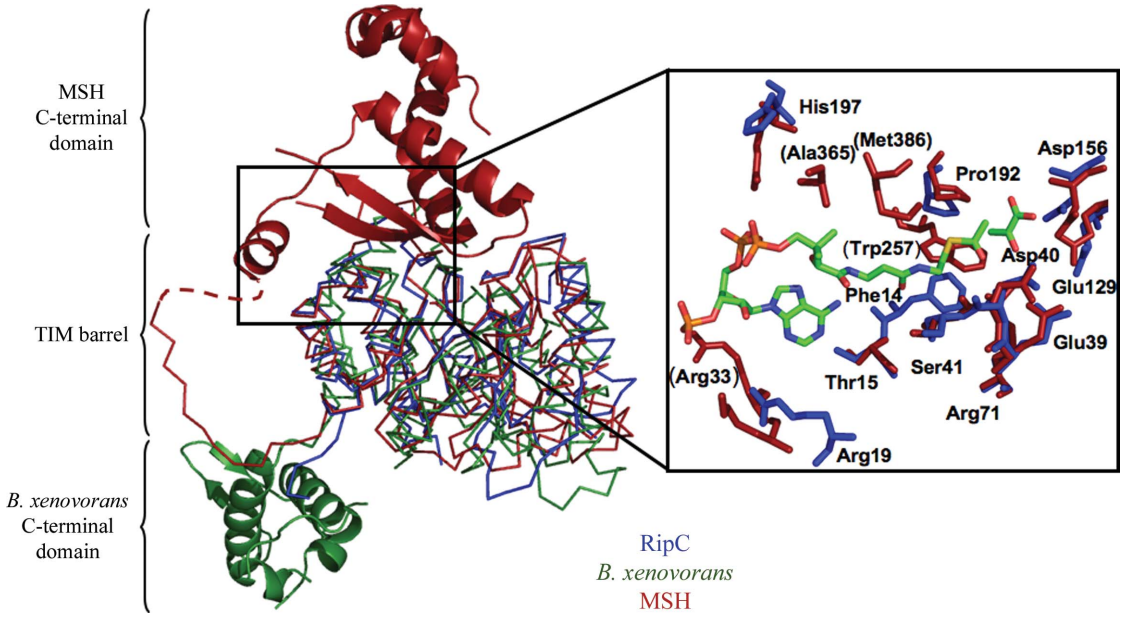

Figure 3
Structural overlay of *Y. pestis* RipC (blue), *B. xenovorans* citrate lyase β subunit (green) and *H. volcanii* malate synthase H (MSH, red), in which the TIM barrels superimpose upon one another and are shown in ribbon representation. The C-terminal domains from *B. xenovorans* and *H. volcanii* are shown in cartoon representation. The dotted line connecting the TIM barrel to the C-terminal domain in MSH suggests a possible intramonomer interaction, although an intermonomer interaction between the C-terminal domain and an adjacent TIM barrel cannot be ruled out. Expanded region: stick representation of active-site residues that are conserved between RipC (blue) and MSH (red). Additional corresponding conserved residues from MSH that are missing from the RipC structure are depicted in parentheses. Acetyl-CoA and pyruvate from MSH are represented as stick models, with C atoms in green, N atoms in blue, O atoms in red, S atoms in yellow and P atoms in orange.

ADP moiety of CoA; although this region (α1) of RipC is unbuilt, sequence alignment reveals a conserved positively charged residue pair Arg19–Arg22 that could potentially facilitate this interaction. Finally, Arg236 in MSH, which forms an electrostatic interaction with the diphosphate arm of CoA, could be compensated by His197 from RipC.

In the *H. volcanii* MSH structure, a two-stranded β-sheet from the C-terminal domain contributes several hydrophobic interactions (*i.e.* Ala365 and Met386) to the pantothenate arm of acetyl-CoA by 'clamping' down to seal off the top of the TIM barrel (Fig. 3). The secondary-structure prediction for the C-terminal RipC domain is similar to the known structure of the C-terminal MSH domain, suggesting that a similar 'clamping' effect may be conserved in RipC with the corresponding residues Gly254 and Met260, as indicated in Fig. 2.

4. Conclusions

The crystal structure of RipC from *Y. pestis*, solved by SAD and refined to 2.45 Å resolution, reveals a canonical TIM barrel and a conserved quaternary arrangement observed in other annotated citrate lyase β subunit homologs as well as *H. volcanii* malate synthase H. Furthermore, sequence and structure comparisons suggest that the top of the TIM barrel and a C-terminal domain, which may belong to its own or an adjacent monomer, comprises the putative active site of RipC. While RipC may not function as a citrate lyase β subunit owing to the absence of the α and γ subunits, it is proposed to still bind a CoA moiety. Within the context of the *rip* operon, RipA has been shown to exhibit acyl-CoA transferase activity (Torres *et al.*, 2011) and RipB is a predicted enoyl-CoA hydrolase; as such, the Rip proteins may be involved in a pathway yielding either a CoA derivative or a carboxylic acid to combat and survive oxidative damage by post-activated macrophages. Possible scenarios include the production of (i) acetyl-CoA, which is a metabolic precursor in fatty-acid biosynthesis for cell-wall fortification (Melching & Vas, 1971) and also can act as an NO sink (Roediger, 2001; Roediger & Babidge, 2000), and/or (ii) butyrate, which has been shown to suppress INF-γ-mediated induction of macrophage-produced NO (Kim *et al.*, 2004). Additional functional and biochemical studies are needed to further characterize the Rip proteins and their final product in order to ultimately elucidate the *rip*-mediated pathogenicity pathway.

This work was supported by grants from the National Institutes of Health (PSWRCE award AI-65359, PI: Alan Barbour, subaward to CWG and Northeast Biodefense Center U54-AI057158-Lipkin, and AI055621 awarded to JBB). The Berkeley Center for Structural Biology is supported in part by the National Institutes of Health, National Institute of General Medical Sciences and the Howard Hughes Medical Institute. The Advanced Light Source is supported by the Director, Office of Science, Office of Basic Energy Sciences of the US Department of Energy under Contract No. DE-AC02-05CH11231.

References

Adams, P. D. *et al.* (2010). *Acta Cryst.* D**66**, 213–221.
Anstrom, D. M., Kallio, K. & Remington, S. J. (2003). *Protein Sci.* **12**, 1822–1832.
Bott, M. & Dimroth, P. (1994). *Mol. Microbiol.* **14**, 347–356.
Bracken, C. D., Neighbor, A. M., Lamlenn, K. K., Thomas, G. C., Schubert, H. L., Whitby, F. G. & Howard, B. R. (2011). *BMC Struct. Biol.* **11**, 23.
Butler, T. (2009). *Clin. Infect. Dis.* **49**, 736–742.
Chen, V. B., Arendall, W. B., Headd, J. J., Keedy, D. A., Immormino, R. M., Kapral, G. J., Murray, L. W., Richardson, J. S. & Richardson, D. C. (2010). *Acta Cryst.* D**66**, 12–21.
Cole, C., Barber, J. D. & Barton, G. J. (2008). *Nucleic Acids Res.* **36**, W197–W201.
DeLano, W. L. (2002). *PyMOL*. http://www.pymol.org.
Emsley, P., Lohkamp, B., Scott, W. G. & Cowtan, K. (2010). *Acta Cryst.* D**66**, 486–501.
Goulding, C. W., Bowers, P. M., Segelke, B., Lekin, T., Kim, C.-Y., Terwilliger, T. C. & Eisenberg, D. (2007). *J. Mol. Biol.* **365**, 275–283.
Heesemann, J., Sing, A. & Trülzsch, K. (2006). *Curr. Opin. Microbiol.* **9**, 55–61.
Kanao, T., Fukui, T., Atomi, H. & Imanaka, T. (2002). *Eur. J. Biochem.* **269**, 3409–3416.
Kim, H.-S., Whang, S.-Y., Woo, M.-S., Park, J.-S., Kim, W.-K. & Han, I.-O. (2004). *J. Neuroimmunol.* **151**, 85–93.
Krissinel, E. & Henrick, K. (2007). *J. Mol. Biol.* **372**, 774–797.
Laskowski, R. A., MacArthur, M. W., Moss, D. S. & Thornton, J. M. (1993). *J. Appl. Cryst.* **26**, 283–291.
Lee, B. & Richards, F. M. (1971). *J. Mol. Biol.* **55**, 379–400.
Melching, L. & Vas, S. I. (1971). *Infect. Immun.* **3**, 107–115.
Otwinowski, Z. & Minor, W. (1997). *Methods Enzymol.* **276**, 307–326.
Pujol, C., Grabenstein, J. P., Perry, R. D. & Bliska, J. B. (2005). *Proc. Natl Acad. Sci. USA*, **102**, 12909–12914.
Roediger, W. E. (2001). *Nitric Oxide*, **5**, 83–87.
Roediger, W. E. & Babidge, W. J. (2000). *Mol. Cell. Biochem.* **206**, 159–167.
Roy, A., Kucukural, A. & Zhang, Y. (2010). *Nature Protoc.* **5**, 725–738.
Schneider, K., Kästner, C. N., Meyer, M., Wessel, M., Dimroth, P. & Bott, M. (2002). *J. Bacteriol.* **184**, 2439–2446.
Smith, C. V., Huang, C.-C., Miczak, A., Russell, D. G., Sacchettini, J. C. & Höner zu Bentrup, K. (2003). *J. Biol. Chem.* **278**, 1735–1743.
Torres, R., Swift, R. V., Chim, N., Wheatley, N., Lan, B., Atwood, B. R., Pujol, C., Sankaran, B., Bliska, J. B., Amaro, R. E. & Goulding, C. W. (2011). *PLoS One*, **6**, e25084.
Van Duyne, G. D., Standaert, R. F., Karplus, P. A., Schreiber, S. L. & Clardy, J. (1993). *J. Mol. Biol.* **229**, 105–124.